# Design of Nonlinear Droop Control in DC Microgrid for Desired Voltage Regulation and Current Sharing Accuracy

Yaoyao Zhang, Xiaohui Qu, *Senior Member, IEEE*, Maodong Tang, Ruoyu Yao, and Wu Chen, *Senior Member, IEEE*

***Abstract*— It is well known that there is a design tradeoff between voltage regulation and load current sharing in conventional linear droop control for several parallel-connected distributed sources in a DC microgrid. To improve both performance areas, this article proposes a design method to identify the nonlinear droop curve coefficient with the desired bus voltage regulation and current sharing accuracy in a specified heavy load range, while a linear droop function with a negative droop resistance is used to tighten the bus voltage regulation in the light load range. The design procedure of load boundary and the effect of negative droop resistances on the system stability are analyzed in detail. Also, a boost-up and curve-fitting method can further improve the voltage regulation and achieve smooth transition between light load and heavy load. In this way, no additional voltage compensation loop is needed. Two parallel-connected DC converters are finally built to verify the theoretical analysis.**

***Index Terms*— DC microgrid, voltage regulation, load current sharing, nonlinear droop control, curve fitting.**

## I. Introduction

CURRENTLY, renewable sources account for an increasing proportion of the total electricity generation in the world. Meanwhile, more and more DC equipments are connected to the grid, such as DC-powered data centers, LED lighting systems, electric vehicle charging stations, and so on. The DC grid is simpler and more efficient considering DC ports of both the source and the load [1], [2]. Therefore, the DC grid becomes popular in recent years. Fig. 1 shows a typical configuration of DC microgrid including multiple solar arrays, loads, and the energy storage station [3], [4]. With different DC voltage levels of sources and loads, interfacing converters need to connect a single DC bus for sources and loads.

Manuscript received September 3, 2020; revised December 6, 2020; accepted January 3, 2021. Date of publication January 8, 2021; date of current version March 11, 2021. This work was supported in part by the National Key Research and Development Program of China under Grant 2018YFB0904100 and in part by the Science and Technology Project of State Grid under Grant SGHB0000KXJS1800685. This article was recommended by Guest Editor Chi K. Tse. *(Corresponding author: Xiaohui Qu.)*

The authors are with the School of Electrical Engineering, Southeast University, Nanjing 210096, China, and also with the Jiangsu Key Laboratory of Smart Grid Technology and Equipment, Nanjing 210096, China (e-mail: xhqu@seu.edu.cn).

Color versions of one or more figures in this article are available at https://doi.org/10.1109/JETCAS.2021.3049810.

Digital Object Identifier 10.1109/JETCAS.2021.3049810

When multiple sources are paralleled into a DC bus, the bus voltage regulation and load sharing accuracy become crucial issues due to different output impedances of converters and line resistances among different converters and the DC bus [5]–[7]. To achieve a tight voltage regulation and an accurate load current sharing, there are some existing methods, which can be classified into centralized and decentralized methods [8], [9]. It is well-known that centralized methods adopt one central controller to adjust the bus voltage and send the same current sharing signals to other converters for power balance [10]–[12]. However, if the central controller fails to run, the DC microgrid will collapse. Besides, the precise communication link is of most importance in the centralized method. To save the communication link and improve system reliability, decentralized methods are expected to find more and more applications, where the droop control is a popular method to construct relatively large virtual resistances in the circuit, thus reducing the load imbalance among different sources [13]–[17]. Obviously, the large droop resistances will make the bus voltage drop even below the minimum bus voltage limit. Some works use hierarchical control by increasing the voltage reference to compensate the bus voltage drop [18]–[20]. But the hierarchical control still needs communication feedback and increases the system complexity. So it is challenging for the linear droop control to achieve good performances for both bus voltage regulation and load sharing.

Considering a practical light loading condition, the output current of each source converter is well below the current limit and the accuracy of load sharing is not an issue for this case. Then the droop resistance can be designed small to permit a tight bus voltage regulation. At heavy load conditions, the interfacing converters suffer almost the full ratings and a small current imbalance may cause over-loading or even failure of some converters. Thus, the droop resistance at heavy loads is expected to be large enough to improve load sharing accuracy. Based on these considerations, some nonlinear droop control methods have been proposed to satisfy the requirements of both load sharing and bus voltage regulation. Reference [21] uses an inverse parabolic function to improve the bus voltage regulation at light loads and to permit good current sharing at heavy loads.But it is hard to design the converters with the desired voltage regulation and current sharing accuracy. Reference [22] gives a nonlinear curve to

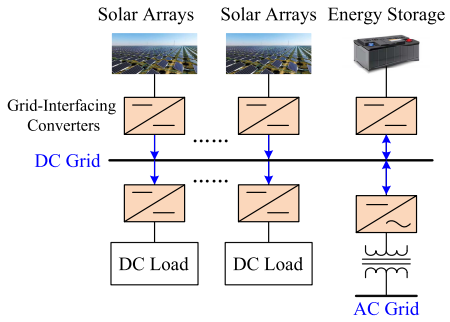


Fig. 1. A typical configuration of a DC microgrid.

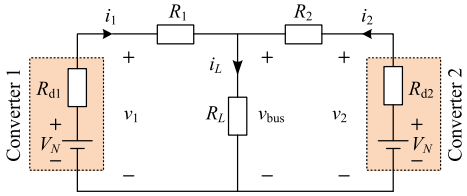


Fig. 2. A simplified DC microgrid with two parallel-connected converters. The shadow area shows equivalent circuits of two converters.

satisfy both requirements, where the droop curve coefficients at different loads are hard and complicated to design. Reference [23] combines droop curves with odd coefficient $n$, i.e., $n = 1,3,5\ldots$, into a polynomial equation as the droop function. However, the bus voltage still exceeds the limit at some loads and a voltage compensation loop is needed.

To solve the above issues, this article proposes a simple design method to identify the nonlinear droop curve coefficient with the desired bus voltage regulation and current sharing accuracy in a specified heavy load range. In the light load range, a linear droop function with a negative droop resistance is proposed to tighten the bus voltage regulation with the allowable current sharing accuracy. In this way, no additional voltage compensation loop is needed. Besides, a boost-up for heavy load and a curve-fitting for the whole load can further improve the bus voltage regulation and ensure the smooth transition between light load and heavy load. The design method can be readily extended to the DC microgrid system with multiple parallel-connected converters. The system stability with the proposed nonlinear droop control is also analyzed considering variations of output load and cable impedances. Finally, two parallel-connected DC converters are built to verify the theoretical analysis.

## II. Fundamental Analysis of Proposed Nonlinear Droop Control Design

To simplify the analysis, a simple DC microgrid system consisting of two parallel-connected converters is applied to feed a load directly, as shown in Fig. 2. Here, $v_{1,2}$ and $i_{1,2}$ are the output voltages and currents of Converter 1 and Converter 2, while $R_1$ and $R_2$ are the line resistances between the converter output port and the load $R_L$. $v_{\text{bus}}$ is the DC bus voltage.

To provide the accurate load sharing performance, the conventional droop control constructs constant droop resistances $R_{\text{d1}}$ and $R_{\text{d2}}$ in series with $R_1$ and $R_2$, and then parallel-connected converters can be further modeled as a

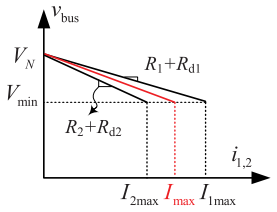


Fig. 3. Bus voltage varying with converter currents under linear droop control.

no-load voltage connected with the droop resistance, as shown in the shadow area of Fig. 2. Usually, the parallel-connected converters are designed at the same no-load voltage $V_N$. Given the acceptable bus voltage minimum $V_{\text{min}}$ and converter output current maximum $I_{\text{imax}}$ ($i = 1$ or 2), the linear droop resistances are designed as

$$R_{\text{di}} = \frac{V_N - V_{\text{min}}}{I_{\text{imax}}}. \tag{1}$$

Then the actual output voltage reference $v_{\text{refi}}$ of converters becomes

$$v_{\text{refi}} = V_N - R_{\text{di}} i_i. \tag{2}$$

When (2) is implemented as the reference of $v_{1,2}$ in the voltage feedback PI controller, the linear droop control makes converter current distributed in (3).

$$\frac{i_1}{i_2} = \frac{R_2 + R_{\text{d2}}}{R_1 + R_{\text{d1}}}. \tag{3}$$

Define the current sharing error $e_I$ as

$$e_I = \left|\frac{i_1 - i_2}{i_1 + i_2}\right| = \left|\frac{R_1 - R_2 + R_{\text{d1}} - R_{\text{d2}}}{R_1 + R_2 + R_{\text{d1}} + R_{\text{d2}}}\right|. \tag{4}$$

From (4), to improve the load sharing accuracy, i.e., to reduce $e_I$, $R_{\text{d1}}$ and $R_{\text{d2}}$ are expected to be close, which means two converters have the identical current rating $I_{\text{max}}$ as shown in Fig. 3. Besides, the larger $R_{\text{d1}}$ and $R_{\text{d2}}$ are, the smaller $e_I$ is. But the linear droop function in (1) has no capability to enhance $R_{\text{d1,2}}$ with the given voltage drop. Therefore, to further reduce $e_I$, the nonlinear droop function with a high curve coefficient is recommended.

### A. Identification of Nonlinear Droop Curve Coefficient for Heavy Load

The general nonlinear droop curve can be expressed as follows [22], where $n$ is the droop curve coefficient and $n > 1$.

$$v_{\text{refi}} = V_N - k_i i_i^n, \text{ where } k_i = \frac{V_N - V_{\text{min}}}{I_{\text{imax}}^n}. \tag{5}$$

Then the equivalent droop resistance $R_{\text{di}}$ working at a load current of $I_i$ can be derived as

$$R_{\text{di}}|_{i_i = I_i} = \left|\frac{dv_{\text{refi}}}{di_i}\right|_{i_i = I_i} = nk_i i_i^{n-1}|_{i_i = I_i}. \tag{6}$$

From (6), equivalent droop resistances vary with the operating load and droop coefficient, as demonstrated in Fig. 4 with the example case of $V_N = 48$ V, $V_{\text{min}} = 46.8$ V, i.e., the voltage regulation ratio $e_V = \frac{V_N - V_{\text{min}}}{V_N} = 2.5$ %, and $I_{1\text{max}} = I_{2\text{max}} = 6$ A. It can be seen that $R_{\text{di}}$ increases as the

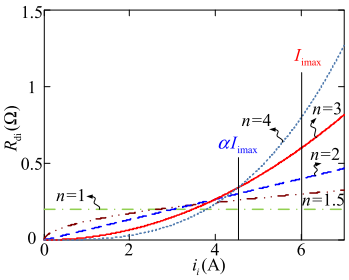


Fig. 4. Droop resistance varying with load current under different droop coefficients, where $n$ = 1 denotes a linear droop control as (1).

operating load increases to $I_{\text{imax}}$, while the higher $n$ makes $R_{\text{di}}$ much larger in a heavy load range of $[\alpha I_{\text{imax}}, I_{\text{imax}}]$. In Fig. 4, $\alpha$ depends on the cross point of different curves. However, in the light load range of $[0, \alpha I_{\text{imax}}]$, the higher $n$ makes $R_{\text{di}}$ much smaller and the linear droop of $n = 1$ has the best current sharing accuracy performance in some light loads. Therefore, a proper $n$ needs to be designed to satisfy the requirement of load current sharing accuracy in a heavy load range of $[\alpha I_{\text{imax}}, I_{\text{imax}}]$.

By (4), the current sharing index $e_I$ decreases with the incremental $R_{\text{di}}$. Therefore, if (5) is well implemented in a heavy load, the worst case, i.e., the maximum $e_{I_{\text{max}}}$, will not occur at $I_{\text{imax}}$, but an interim load. From Fig. 4, if $e_I$ at the current of $\alpha I_{\text{imax}}$ is smaller than $e_{I_{\text{max}}}$ and $n > 1$, $e_I$ will not exceed $e_{I_{\text{max}}}$ during $[\alpha I_{\text{imax}}, I_{\text{imax}}]$. In this way, a minimum $n$ can be determined in the heavy load.

Taking two parallel-connected converters as an example, according to Kirchhoff's voltage law in Fig. 2, we have

$$v_{\text{bus}} = V_N - k_1 i_1^n - R_1 i_1 = V_N - k_2 i_2^n - R_2 i_2. \tag{7}$$

Then it can be further derived as

$$k_1 i_1^n + R_1 i_1 = k_2 i_2^n + R_2 i_2. \tag{8}$$

According to (4), the maximum $e_{I_{\text{max}}}$ should be satisfied. Thus

$$|i_1 - i_2| \le e_{I_{\text{max}}}(i_1 + i_2). \tag{9}$$

By solving (8) and (9), the expressions in the two cases can be obtained.

1) If $i_1 \le i_2$, then $i_2 \le \gamma i_1$.

$$\begin{cases} i_1 \le \sqrt[n-1]{\dfrac{R_2\gamma - R_1}{k_1 - k_2\gamma^n}} \text{ if } k_1 - k_2\gamma^n > 0 \\ i_1 \ge \sqrt[n-1]{\dfrac{R_1 - R_2\gamma}{k_2\gamma^n - k_1}} \text{ if } k_1 - k_2\gamma^n < 0, \end{cases} \tag{10}$$

where $\gamma = \frac{1+e_{I_{\text{max}}}}{1-e_{I_{\text{max}}}}$.

2) If $i_1 > i_2$, then $i_1 \le \gamma i_2$

$$\begin{cases} i_2 \le \sqrt[n-1]{\dfrac{R_1\gamma - R_2}{k_2 - k_1\gamma^n}} \text{ if } k_2 - k_1\gamma^n > 0 \\ i_2 \ge \sqrt[n-1]{\dfrac{R_2 - R_1\gamma}{k_1\gamma^n - k_2}} \text{ if } k_2 - k_1\gamma^n < 0. \end{cases} \tag{11}$$

Selection of case 1 and case 2 is determined by judging the real solutions of $i_1$ and $i_2$ with the given parameters.

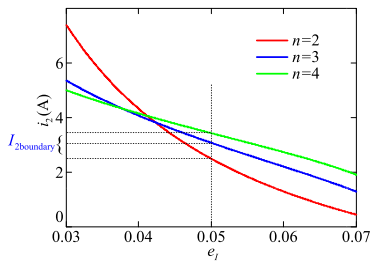


(a) $R_1$ = 0.3 Ω and $R_2$ = 0.35 Ω

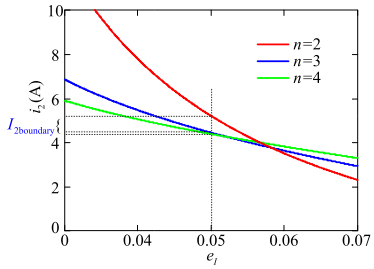


(b) $R_1$ = 0.3 Ω and $R_2$ = 0.37 Ω

Fig. 5. Solved $i_2$ varying with $e_I$ at the different $n$ for two cases.

To guarantee $e_I \le e_{I_{\text{max}}}$ during $[\alpha I_{\text{imax}}, I_{\text{imax}}]$, the solved $I_{1\text{boundary}}$ or $I_{2\text{boundary}}$ with the $n^{\text{th}}$ nonlinear droop function in (10) or (11) must follow

$$\begin{aligned} I_{1\text{boundary}} &\le \alpha I_{1\text{max}} \text{ for case 1, or} \\ I_{2\text{boundary}} &\le \alpha I_{2\text{max}} \text{ for case 2.} \end{aligned} \tag{12}$$

With the criteria of (12), the minimum $n$ can be uniquely determined at the given $e_{I_{\text{max}}}$. For example, the converter is designed as Fig. 4. The desired bus voltage regulation is ±2.5%, and $e_{I_{\text{max}}}$ is set as 5%. Then $\gamma \approx 1.1$. If $R_1 = 0.3\ \Omega$, and $R_2 = 0.32\ \Omega$, there is no real solution of $I_{1\text{boundary}}$ and $I_{2\text{boundary}}$ for both cases, which means a linear droop control is enough with $e_I = 2\%$ by (4). If $R_2$ is 0.35 Ω, by solving (10) and (11), (11) is available with real solutions $I_{2\text{boundary}}$ with different $n$ as shown in Fig. 5(a). It can be seen that the smaller $n$ relates to the smaller $I_{2\text{boundary}}$, which is consistent with curves in the light load range in Fig. 4. In the range of $[0, I_{2\text{boundary}}]$, the linear curve with $n = 1$ has a smaller $e_I = 4.8\%$. If $R_2$ is 0.37 Ω, (11) is available as shown in Fig. 5(b), where a higher $n$ generates a smaller $I_{2\text{boundary}}$ to satisfy (12). From Fig. 5(b), if $\alpha$ is set as 0.75, the minimum $n = 3$ is required.

### *B. Negative Linear Droop Resistance for Light Load*

In the range of $[0, \alpha I_{\text{imax}}]$, the linear droop control is usually used to permit the desired voltage regulation. From Fig. 4, the current sharing accuracy of the linear droop control is better than other curves with large droop coefficients in the light load range, although $e_I$ may exceed the required $e_{I_{\text{max}}}$. By (4) and $i_1 + i_2 = i_L$, we have

$$i_{1,2} = \frac{i_L(1 \pm e_I)}{2}. \tag{13}$$

Taking the above example, $R_1 = 0.3\ \Omega$ and $R_2 = 0.37\ \Omega$. $\alpha$ is set as 0.75 and $I_{1,2\text{max}} = 6$ A. During [9 A, 12 A] of the load, a third droop curve is used to permit the voltage

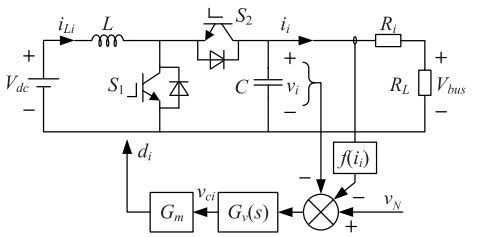


Fig. 6. The schematic of bidirectional buck/boost converter with droop control.

regulation below 2.5% and the current sharing accuracy below 5% from Section II-A. During $i_L \in [0\text{ A}, 9\text{ A}]$, the linear droop curve is used to permit the voltage regulation below 2.5%, whilst the current sharing accuracy error $e_I$ can be calculated as 6.5%. By (13), if $i_L = 9$ A, the output currents of two converters are about 4.8 A and 4.2 A, which are far below converter ratings. Therefore, to further decrease the voltage regulation at the light load range, we can decrease the linear droop resistance even up to a negative resistance. Obviously, the smaller or even negative droop resistance will lead to a large $e_I$. By (13), the allowable $e_I$ can be obtained as

$$e_{I_{\text{allow}}} = \frac{2I_{\text{imax}}}{i_L} - 1. \tag{14}$$

So we can define a new linear droop resistance $R'_{\text{di}}$ satisfying (14).

$$R'_{\text{di}} = \beta \cdot R_{\text{di}}, \tag{15}$$

where $0 < \beta \leq 1$ denotes a smaller positive droop resistance and $\beta < 0$ denotes a negative droop resistance. It is apparent that a negative droop resistance will have a tighter voltage regulation and lead to a larger $e_I$.

Also, a negative droop resistance may affect converter stability performance. Taking a bidirectional buck/boost converter as an example, as shown in Fig. 6, the output voltage reference is modified by the droop function $f(i_i) = R'_{\text{di}} i_i$. Here, $G_v(s)$ is the transfer function of the PI controller in the voltage loop, and $G_m$ is the modulation function of the duty cycle. From Fig. 6, the small-signal block diagram of the whole converter is thus demonstrated in Fig. 7, where $G_{vd}(s) = \frac{\Delta v_i(s)}{\Delta d_i(s)}|_{\Delta i_i(s),\Delta v_{dc}(s)=0}$, $G_{vv}(s) = \frac{\Delta v_i(s)}{\Delta v_{dc}(s)}|_{\Delta i_i(s),\Delta d_i(s)=0}$, $G_{id}(s) = \frac{\Delta i_L(s)}{\Delta d_i(s)}|_{\Delta i_i(s),\Delta v_{dc}(s)=0}$, and $G_{ii}(s) = \frac{\Delta i_L(s)}{\Delta i_i(s)}|_{\Delta v_{dc}(s),\Delta d_i(s)=0}$. $Z_{in}(s)$ and $Z_o(s)$ are the input and output impedances of the converter, separately.

To analyze the stability of the converter, the open-loop gain $T(s)$ is required. In Fig. 7, there are two loops with loop gains defined as $T_v(s)$ and $T_i(s)$. By the control theory, the loop gain $T(s)$ can be expressed as

$$T(s) = \frac{T_v(s)}{1+T_i(s)}, \tag{16}$$

where,

$$T_v(s) = G_v(s)G_m G_{vd}(s), \text{ and} \tag{17}$$

$$T_i(s) = G_v(s)G_m G_{vd}(s)\beta R_{\text{di}} \frac{1}{Z_o(s)}. \tag{18}$$

Using the PI controller, $G_v(s) = k_{\text{pv}} + \frac{k_{\text{iv}}}{s}$, and $k_{\text{pv}}$ and $k_{\text{iv}}$ are proportional and integral coefficients. The modulation function

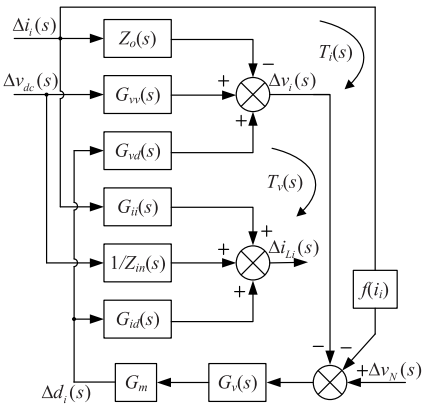


Fig. 7. The small-signal control block diagram of Fig. 6 using the droop control function $f(i_i)$.

$G_m$ is usually expressed as $\frac{1}{V_M}$, where $V_M$ is the amplitude of the ramp signal. To achieve the transfer function $G_{vd}(s)$ and $Z_o(s)$, the state space equations can be established as follows.

$$\begin{cases} L\dfrac{d\Delta i_{Li}}{dt} = \Delta v_{dc} + V_i \Delta d_i - (1 - D_i)\Delta v_i \\ C\dfrac{d\Delta v_i}{dt} = (1 - D_i)\Delta i_{Li} - I_{Li}\Delta d_i - \Delta i_i, \end{cases} \tag{19}$$

where $D_i$ represents the steady-state duty cycle of $S_1$ in the $i^{\text{th}}$ converter. From (19), we have

$$Z_o(s) = \frac{Ls}{LCs^2 + \frac{L}{R_L+R_i}s + (1 - D_i)^2}, \text{ and}$$
$$G_{vd}(s) = \frac{V_{dc} - I_{Li}Ls}{LCs^2 + \frac{L}{R_L+R_i}s + (1 - D_i)^2}. \tag{20}$$

Substituting (20) into (17) and (18), $T(s)$ can be plotted in bode curves, as shown in Fig. 8. The converter parameters are listed in Table I in Section IV. From Fig. 8, it shows that a large negative droop resistance corresponds to a large phase margin at the crossover frequency $f_c$. When $\beta$ becomes $-1.5$ or $-2$, the converter is even not stable. Therefore, we choose $\beta$ of $-0.7$ to have a phase margin of 37.7°. For the example case, the new linear droop control has a tight voltage regulation of 0.44% and the current sharing accuracy of 17.9%, not exceeding $e_{I_{\text{allow}}}$ of 33.3%.

### *C. Curve Fitting Method for Smooth Transition*

According to the above discussion, a segmented curve is utilized to realize the negative linear droop resistance, i.e., $n = 1$, at light loads of $[0, \alpha I_{\text{imax}}]$ and a larger nonlinear positive droop resistance, e.g., $n = 3$, at heavy loads of $[\alpha I_{\text{imax}}, I_{\text{imax}}]$, as the red and blue solid curves shown in Fig. 9. Usually, the least square curve fitting algorithm is required to combine these two curves. Here, to realize the smooth transition, a boost-up of the nonlinear curve reaching the end of the linear curve can be adopted further reducing the voltage drop at heavy loads, as the brown curve in Fig. 9. The brown curve can be expressed as

$$v_{\text{refi}} = V_N + \sum_{m=1}^{n} k_m i_i^m, \tag{21}$$

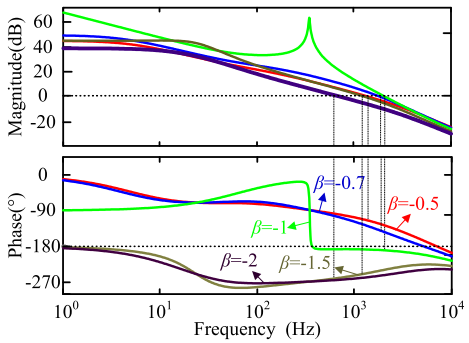


Fig. 8. Magnitude and phase curves of $T(s)$ under different $\beta$.

TABLE I
EXPERIMENTAL PARAMETERS

| Parameter | Value |
|---|---|
| Nominal voltage $V_N$ | 48 V |
| Nominal current $I_N$ | 6 A |
| Input voltage $V_{dc}$ | 36 V |
| Line resistance $R_1$, $R_2$ | 0.3Ω, 0.37Ω |
| Switching frequency $f_s$ | 50 kHz |
| Inductor $L$ | 150 $\mu$H |
| Output capacitor $C$ | 470 $\mu$F |

where $k_m$ represents polynomial fitting coefficients, and $n$ indicates the highest order of the fitting curve. By (21), the droop function becomes

$$f(i_i) = \sum_{m=1}^{n} k_m i_i^m. \tag{22}$$

It can be readily implemented in Fig. 6.

### D. Extension to Multiple Parallel-Connected Converters

If the DC microgrid system has multiple parallel-connected converters, the above analysis is still available. In such a case, output currents for $N$ converters can be expressed as

$$\begin{cases} i_1 = \dfrac{V_N R_2' R_3' \cdots R_N'}{R_1' R_2' \cdots R_N' + R_L \sum_{j=1}^{N} \frac{R_1' R_2' \cdots R_N'}{R_j}} \\ i_2 = \dfrac{V_N R_1' R_3' \cdots R_N'}{R_1' R_2' \cdots R_N' + R_L \sum_{j=1}^{N} \frac{R_1' R_2' \cdots R_N'}{R_j}} \\ \cdots \\ i_N = \dfrac{V_N R_1' R_2' \cdots R_{N-1}'}{R_1' R_2' \cdots R_N' + R_L \sum_{j=1}^{N} \frac{R_1' R_2' \cdots R_N'}{R_j}}, \end{cases} \tag{23}$$

where $R_j' = R_j + R_{\mathrm{dj}}$ and $j \in [1, N]$. $i_p$ and $i_q$ are defined as the maximum output current and the minimum output current among $N$ converters, i.e., $i_p = \max\{\mathrm{i_1}, \mathrm{i_2}, \cdots \mathrm{i_N}\}$ and $i_q = \min\{\mathrm{i_1}, \mathrm{i_2}, \cdots \mathrm{i_N}\}$.

Following (4), the maximum current sharing error $e_I$ between $i_p$ and $i_q$ can be given as

$$e_I = \left| \frac{i_p - i_q}{i_p + i_q} \right| = \left| \frac{R_q - R_p + R_{\mathrm{dq}} - R_{\mathrm{dp}}}{R_q + R_p + R_{\mathrm{dq}} + R_{\mathrm{dp}}} \right|. \tag{24}$$

If the maximum current sharing error and voltage regulation satisfy the desired requirements, the output currents and voltages of the other converters must be within the desired ranges. Therefore, with (24) and the acceptable bus voltage minimum $V_{\min}$, the nonlinear droop curve could be designed according to Section II-A, B, and C.

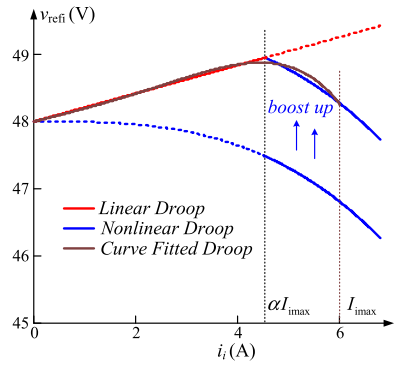


Fig. 9. Segmented droop control curves and their fitted curve.

## III. STABILITY ANALYSIS

Although the design of negative droop resistance has considered the system stability issue in Section II-B, the analysis is based on the converter with the constant output power and cable resistances. In practice, the converter may operate at different power levels, and the cable resistances and inductances also vary with temperature and time, as shown in Fig. 10. To check the system stability in such a range of operation conditions, the state variable vector of the system can be got as $\mathbf{x} = [\Delta v_1\ \Delta v_2\ \Delta i_1\ \Delta i_2\ \Delta i_{L1}\ \Delta i_{L2}\ \Delta v_{c1}\ \Delta v_{c2}]^T$.

From Fig. 6, it gives

$$v_{ci} = [v_N + f(i_i) - v_i] \left( k_{\mathrm{pv}} + \frac{k_{\mathrm{iv}}}{s} \right). \tag{25}$$

Upon differentiating both sides of equation in (25), we get

$$\frac{dv_{ci}}{dt} = k_{\mathrm{pv}} \left[ f(i_i)' \frac{di_i}{dt} - \frac{dv_i}{dt} \right] + k_{\mathrm{iv}} [v_N + f(i_i) - v_i], \tag{26}$$

where $f(i_i)' = \sum_{m=1}^{n} m k_m i_i^{m-1}$.

According to Fig. 10, the state equations of a two-converter based microgrid can be linearized by using (19) and (26). It gives

$$\begin{aligned}
\frac{dx_1}{dt} &= -\frac{1}{C} x_3 + \frac{D_1'}{C} x_5 - \frac{I_{L1} G_m}{C} x_7, \\
\frac{dx_2}{dt} &= -\frac{1}{C} x_4 + \frac{D_2'}{C} x_6 - \frac{I_{L2} G_m}{C} x_8, \\
\frac{dx_3}{dt} &= \frac{1}{L_{l1}} x_1 - \frac{R_1 + R_L}{L_{l1}} x_3 - \frac{R_L}{L_{l1}} x_4, \\
\frac{dx_4}{dt} &= \frac{1}{L_{l2}} x_2 - \frac{R_L}{L_{l2}} x_3 - \frac{R_2 + R_L}{L_{l2}} x_4, \\
\frac{dx_5}{dt} &= -\frac{D_1'}{L_1} x_1 + \frac{V_1 G_m}{L_1} x_7, \\
\frac{dx_6}{dt} &= -\frac{D_2'}{L_2} x_2 + \frac{V_2 G_m}{L_2} x_8, \\
\frac{dx_7}{dt} &= -(k_{\mathrm{pv}} \frac{dx_1}{dt} + k_{\mathrm{iv}} x_1) + f(i_1)' (k_{\mathrm{pv}} \frac{dx_3}{dt} + k_{\mathrm{iv}} x_3), \\
\frac{dx_8}{dt} &= -(k_{\mathrm{pv}} \frac{dx_2}{dt} + k_{\mathrm{iv}} x_2) + f(i_2)' (k_{\mathrm{pv}} \frac{dx_4}{dt} + k_{\mathrm{iv}} x_4).
\end{aligned} \tag{27}$$

By (27), the state equations can be expressed as

$$\dot{x} = Ax. \tag{28}$$

Then the state matrix $A$ can be derived as shown in (29), at the bottom of the next page. The eigenvalues of matrix

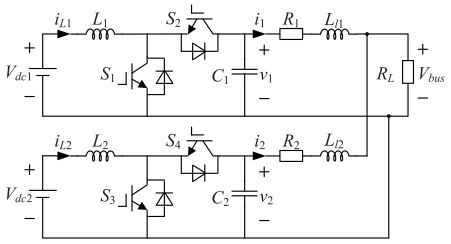


Fig. 10. The simplified DC microgrid model for stability analysis.

$A$ can be calculated by the state-space equation eigenvalue analysis. If all the eigenvalues in matrix $A$ are located in the left half-plane of $s$ domain, the system is stable under the small disturbance near the steady-state operating point [24], [25].

With the above analysis, the root loci of the system eigenvalues can be plotted under different power and cable parameters, as shown in Fig. 11. If the system operates at the fixed cable parameters, i.e., $R_1 = 0.3\ \Omega$, $R_2 = 0.37\ \Omega$, and $L_{l1} = L_{l2} = 300\ \mu$H, Fig. 11(a) demonstrates the root locus of eigenvalues in a power range from 0 to the full load of 600 W, where all eigenvalues locate in the left half-plane. Thus, the system is stable in the designed power range. With the increasing power, the eigenvalues move to the right half-plane, which indicates the system stability margin becomes small. Fig. 11(b) gives the root locus of the eigenvalues with one increasing cable resistance $R_2$ from 0.1 $\Omega$ to 1.5 $\Omega$ and $R_1$ keeping as 0.3 $\Omega$ at a fixed load rating of 600 W as an example. From Fig. 11(b), all eigenvalues locate in the left half-plane and move left with the increasing $R_2$, which indicates a stable system in the variation of cable resistance. The root locus of eigenvalues, shown in Fig. 11(c), is obtained by varying the cable inductance from 20 $\mu$H to 650 $\mu$H, while $R_1 = 0.3\ \Omega$, $R_2 = 0.37\ \Omega$, and the power is fixed at 600 W. It should be noticed that the real parts of some eigenvalues reach zero when the cable inductance rises to 610 $\mu$H. If the cable inductance continues to increase, some eigenvalues go into the right plane and the system becomes unstable. Therefore, the cable inductances can not be designed so large to avoid the unstable system.

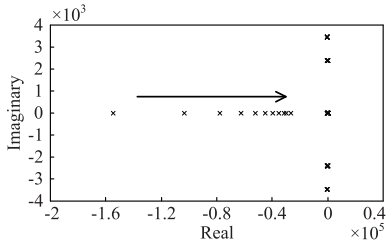


(a) with the increasing power.

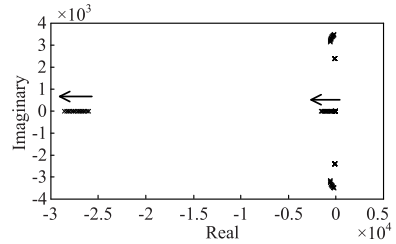


(b) with the increasing cable resistance $R_2$.

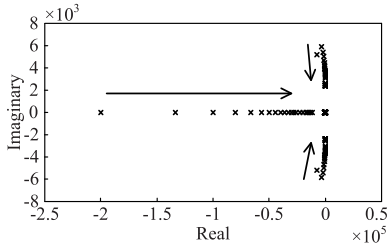


(c) with the increasing cable inductance $L_{li}$.

Fig. 11. Root loci of system eigenvalues with (a) the increasing power, (b) the increasing cable resistance and (c) the increasing cable inductance.

## IV. Experimental Verification

To verify the above analysis, two same bidirectional buck/boost converters with each power level of about 300 W are built and connected in parallel to form a simple DC microgrid. The experimental parameter is shown in Table I. The DC input voltage of two converters is 36 V and the no-load output voltage $V_N$ is set as 48 V. The maximum output current $I_{\max}$ of each converter is 6 A. The desired voltage regulation is $\pm 2.5\%$ and the maximum current sharing accuracy error is 5%. Line resistances are set as $R_1 = 0.3\ \Omega$ and $R_2 = 0.37\ \Omega$. The fitted droop control function $f(i_i)$ in Fig. 9 is $f(i_i) = 0.1887 i_i + 0.00593 i_i^3 - 0.000278 i_i^5$, where converters 1 and 2 have the same parameters and curves. The control PI parameters of each converter are as follows: $k_{\rm pv} = 0.5$, and $k_{\rm iv} = 200$. $\alpha$ is set as 0.75 and $\beta$ is set as

$$A = \begin{bmatrix} 0 & 0 & -\frac{1}{C} & 0 & \frac{D_1'}{C} & 0 & -\frac{I_{L1}G_m}{C} & 0 \\ 0 & 0 & 0 & -\frac{1}{C} & 0 & \frac{D_2'}{C} & 0 & -\frac{I_{L2}G_m}{C} \\ \frac{1}{L_{l1}} & 0 & -\frac{R_1+R_L}{L_{l1}} & -\frac{R_L}{L_{l1}} & 0 & 0 & 0 & 0 \\ 0 & \frac{1}{L_{l2}} & -\frac{R_L}{L_{l2}} & -\frac{R_2+R_L}{L_l 2} & 0 & 0 & 0 & 0 \\ -\frac{D_1'}{L_1} & 0 & 0 & 0 & 0 & 0 & \frac{V_1 G_m}{L_1} & 0 \\ 0 & -\frac{D_2'}{L_2} & 0 & 0 & 0 & 0 & 0 & \frac{V_2 G_m}{L_2} \\ \frac{k_{\rm pv} f(i_1)'}{L_{l1}} - k_{\rm iv} & 0 & a_{73} & -\frac{k_{\rm pv} f(i_1)' R_L}{L_{l1}} & -\frac{k_{\rm pv} D_1'}{C} & 0 & \frac{k_{\rm pv} I_{L1} G_m}{C} & 0 \\ 0 & \frac{k_{\rm pv} f(i_2)'}{L_{l2}} - k_{\rm iv} & -\frac{k_{\rm pv} f(i_2)' R_L}{L_{l2}} & a_{84} & 0 & -\frac{k_{\rm pv} D_2'}{C} & 0 & \frac{k_{\rm pv} I_{L2} G_m}{C} \end{bmatrix},$$

$$\text{where } a_{73} = \frac{k_{\rm pv}}{C} + k_{\rm iv} f(i_1)' - \frac{k_{\rm pv} f(i_1)'(R_1 + R_L)}{L_{l1}} \text{ and } a_{84} = \frac{k_{\rm pv}}{C} + k_{\rm iv} f(i_2)' - \frac{k_{\rm pv} f(i_2)'(R_2 + R_L)}{L_{l2}} \tag{29}$$

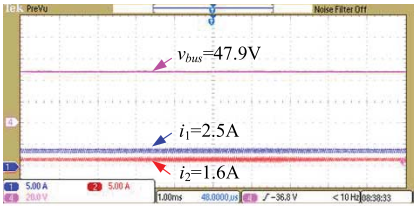


Fig. 12. Waveforms of $v_{\text{bus}}$, $i_1$ and $i_2$ at a light total load of 200 W.

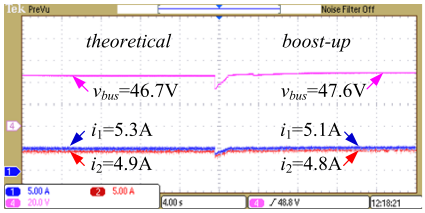


Fig. 13. Waveforms of $v_{\text{bus}}$, $i_1$ and $i_2$ at a heavy load of 480 W with the theoretical 3rd droop coefficient (left) and the boost-up fitted curve in Fig. 9 (right).

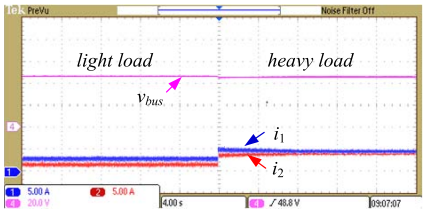


Fig. 14. Dynamic waveforms of $v_{\text{bus}}$, $i_1$ and $i_2$ at a load stepping from 200 W to 480 W.

$-0.7$. The control scheme is carried out in a TMS320F28335 microcontroller.

Fig. 12 shows the experimental waveforms of the bus voltage $v_{\text{bus}}$, converter output currents $i_1$ and $i_2$ at a light total load of about 200 W. Here, with the negative droop resistance, $v_{\text{bus}}$ is measured as 47.9 V and the voltage deviation $e_V$ is calculated as 0.2% far below the limit of $\pm 2.5\%$. The current sharing accuracy $e_I$ can be calculated as 21.9%, which is consistent with the theoretical 17.9%. The difference is caused by the fitted curve, which is not the exactly linear line. Although the experimental $e_I$ is far beyond the required 5%, it is designed below $e_{I_{\text{allow}}}$ of 33.3% by (14). Thus two converters work in the safe current range and show a tight voltage regulation.

When the load is increased to 480 W beyond $\alpha$ of total power 600 W, a higher droop coefficient $n$ of 3 is used. The left side in Fig. 13 shows the experimental waveforms of $v_{\text{bus}}$, $i_1$ and $i_2$ with the theoretical 3rd droop coefficient curve. From the measured $v_{\text{bus}}$, $i_1$ and $i_2$, $e_V$ is calculated as 2.7%, close to the predesigned 2.5%. The small tolerance is usually caused by measurement error. And $e_I$ is measured as 3.9%, satisfying the required 5%. So the 3rd droop coefficient curve is proved to realize the desired voltage regulation and current sharing accuracy in a specified heavy load range. To further tighten the voltage regulation, a boost-up 3rd droop coefficient curve, i.e., the boost-up curve in Fig. 9, is implemented and shows the waveforms on the right side of Fig. 13. Due to the fitted boost-up curve, $e_I$ becomes 3%, a bit different from the initial 3.9%. But the bus regulation can be well improved at 0.8%. So the fitted curve shows good performance in both voltage regulation and current sharing. Fig. 14 also gives the dynamic waveforms with load changing from 200 W to 480 W. The proposed nonlinear droop control scheme ensures a fast and stable system.

## V. Conclusion

To permit a DC microgrid with the desired bus voltage regulation and current sharing accuracy, this article proposes a method to identify the nonlinear droop curve coefficient in a specified heavy load range, while a linear droop control with negative droop resistances is used to tighten the bus voltage regulation under the allowable current sharing accuracy in the light load range. The design procedure of load boundary and the effect of negative droop resistances on the system stability are detailed. Besides, a boost-up and curve-fitting method can further improve the voltage regulation and achieve the smooth transition between light load and heavy load. In this way, no additional voltage compensation loop is needed. The experimental results verify the theoretical analysis well. The method can be readily extended to the DC microgrid with multiple parallel-connected converters.

## References

[1] X. Li *et al.*, "Observer-based DC voltage droop and current feed-forward control of a DC microgrid," *IEEE Trans. Smart Grid*, vol. 9, no. 5, pp. 5207–5216, Sep. 2018.

[2] N. Rashidirad, M. Hamzeh, K. Sheshyekani, and E. Afjei, "An effective method for low-frequency oscillations damping in multibus DC microgrids," *IEEE J. Emerg. Sel. Topics Circuits Syst.*, vol. 7, no. 3, pp. 403–412, Sep. 2017.

[3] M. Kwon and S. Choi, "Control scheme for autonomous and smooth mode switching of bidirectional DC–DC converters in a DC microgrid," *IEEE Trans. Power Electron.*, vol. 33, no. 8, pp. 7094–7104, Aug. 2018.

[4] J. M. Guerrero, P. C. Loh, T.-L. Lee, and M. Chandorkar, "Advanced control architectures for intelligent microgrids—Part II: Power quality, energy storage, and AC/DC microgrids," *IEEE Trans. Ind. Electron.*, vol. 60, no. 4, pp. 1263–1270, Apr. 2013.

[5] X. Lu, J. M. Guerrero, K. Sun, and J. C. Vasquez, "An improved droop control method for DC microgrids based on low bandwidth communication with DC bus voltage restoration and enhanced current sharing accuracy," *IEEE Trans. Power Electron.*, vol. 29, no. 4, pp. 1800–1812, Apr. 2014.

[6] C. Wei, Y. Daopei, C. Jialin, W. Yongzhi, and Y. Yuxing, "The impact of line resistance on load sharing and an improved droop control of DC microgrid," in *Proc. 9th Int. Conf. Power Electron. ECCE Asia (ICPE-ECCE Asia)*, Seoul, South Korea, Jun. 2015, pp. 208–212.

[7] J. Beerten and R. Belmans, "Analysis of power sharing and voltage deviations in droop-controlled DC grids," *IEEE Trans. Power Syst.*, vol. 28, no. 4, pp. 4588–4597, Nov. 2013.

[8] V. Nougain, S. Mishra, and A. K. Pradhan, "MVDC microgrid protection using a centralized communication with a localized backup scheme of adaptive parameters," *IEEE Trans. Power Del.*, vol. 34, no. 3, pp. 869–878, Jun. 2019.

[9] D. Chen, L. Xu, and L. Yao, "DC voltage variation based autonomous control of DC microgrids," *IEEE Trans. Power Del.*, vol. 28, no. 2, pp. 637–648, Apr. 2013.

[10] P. C. Loh, D. Li, Y. K. Chai, and F. Blaabjerg, "Hybrid AC–DC microgrids with energy storages and progressive energy flow tuning," *IEEE Trans. Power Electron.*, vol. 28, no. 4, pp. 1533–1543, Apr. 2013.

[11] H. S. Bidgoli and T. Van Cutsem, "Combined local and centralized voltage control in active distribution networks," *IEEE Trans. Power Syst.*, vol. 33, no. 2, pp. 1374–1384, Mar. 2018.

[12] W. Jiang and B. Fahimi, "Active current sharing and source management in fuel cell–battery hybrid power system," *IEEE Trans. Ind. Electron.*, vol. 57, no. 2, pp. 752–761, Feb. 2010.

[13] M. Mokhtar, M. I. Marei, and A. A. El-Sattar, "An adaptive droop control scheme for DC microgrids integrating sliding mode voltage and current controlled boost converters," *IEEE Trans. Smart Grid*, vol. 10, no. 2, pp. 1685–1693, Mar. 2019.

[14] S. Anand, B. G. Fernandes, and J. Guerrero, "Distributed control to ensure proportional load sharing and improve voltage regulation in low-voltage DC microgrids," *IEEE Trans. Power Electron.*, vol. 28, no. 4, pp. 1900–1913, Apr. 2013.
[15] V. Nasirian, A. Davoudi, F. L. Lewis, and J. M. Guerrero, "Distributed adaptive droop control for DC distribution systems," *IEEE Trans. Energy Convers.*, vol. 29, no. 4, pp. 944–956, Dec. 2014.
[16] P. C. Nakka and M. K. Mishra, "Droop characteristics based damping and inertia emulation of DC link in a hybrid microgrid," *IET Renew. Power Gener.*, vol. 14, no. 6, pp. 1044–1052, Apr. 2020.
[17] N. L. Diaz, T. Dragicevic, J. C. Vasquez, and J. M. Guerrero, "Intelligent distributed generation and storage units for DC microgrids—A new concept on cooperative control without communications beyond droop control," *IEEE Trans. Smart Grid*, vol. 5, no. 5, pp. 2476–2485, Sep. 2014.
[18] N. M. Dehkordi, N. Sadati, and M. Hamzeh, "Robust tuning of transient droop gains based on Kharitonov's stability theorem in droop-controlled microgrids," *IET Gener., Transmiss. Distrib.*, vol. 12, no. 14, pp. 3495–3501, Aug. 2018.
[19] Q. Shafiee, J. M. Guerrero, and J. C. Vasquez, "Distributed secondary control for Islanded microgrids—A novel approach," *IEEE Trans. Power Electron.*, vol. 29, no. 2, pp. 1018–1031, Feb. 2014.
[20] X. Yu, X. She, X. Ni, and A. Q. Huang, "System integration and hierarchical power management strategy for a solid-state transformer interfaced microgrid system," *IEEE Trans. Power Electron.*, vol. 29, no. 8, pp. 4414–4425, Aug. 2014.
[21] F. Chen, R. Burgos, D. Boroyevich, J. C. Vasquez, and J. M. Guerrero, "Investigation of nonlinear droop control in DC power distribution systems: Load sharing, voltage regulation, efficiency, and stability," *IEEE Trans. Power Electron.*, vol. 34, no. 10, pp. 9404–9421, Oct. 2019.
[22] A. Khorsandi, M. Ashourloo, H. Mokhtari, and R. Iravani, "Automatic droop control for a low voltage DC microgrid," *IET Gener., Transmiss. Distrib.*, vol. 10, no. 1, pp. 41–47, Jan. 2016.
[23] P. Prabhakaran, Y. Goyal, and V. Agarwal, "Novel nonlinear droop control techniques to overcome the load sharing and voltage regulation issues in DC microgrid," *IEEE Trans. Power Electron.*, vol. 33, no. 5, pp. 4477–4487, May 2018.
[24] M. Wu and D. D.-C. Lu, "A novel stabilization method of LC input filter with constant power loads without load performance compromise in DC microgrids," *IEEE Trans. Ind. Electron.*, vol. 62, no. 7, pp. 4552–4562, Jul. 2015.
[25] L. Guo, S. Zhang, X. Li, Y. W. Li, C. Wang, and Y. Feng, "Stability analysis and damping enhancement based on frequency-dependent virtual impedance for DC microgrids," *IEEE J. Emerg. Sel. Topics Power Electron.*, vol. 5, no. 1, pp. 338–350, Mar. 2017.

**Yaoyao Zhang** received the B.Eng. degree in electrical engineering from the Nanjing Institute of Technology, Nanjing, China, in 2017. He is currently pursuing the Ph.D. degree in power electronics with the School of Electrical Engineering, Southeast University, Nanjing, China.

His current research interest includes the modeling and stability analysis of dc microgrids.

**Xiaohui Qu** (Senior Member, IEEE) received the B.Eng. and M.Eng. degrees in electrical engineering from the Nanjing University of Aeronautics and Astronautics, Nanjing, China, in 2003 and 2006, respectively, and the Ph.D. degree in power electronics from The Hong Kong Polytechnic University, Hong Kong, in 2010.

From February to May 2009, she was a Visiting Scholar with the Center for Power Electronics Systems, Virginia Tech, VA, USA. Since 2010, she has been with the School of Electrical Engineering, Southeast University, China, where she is currently a Full Professor with research focus on power electronics. From January 2015 to January 2016, she was a Visiting Scholar with the Center of Reliable Power Electronics (CORPE), Aalborg University, Denmark. Her current research interests include LED lighting systems, wireless power transfer, and power electronics reliability.

Dr. Qu received the Outstanding Reviewer Award and the Prize Paper Award from the IEEE TRANSACTIONS ON POWER ELECTRONICS in 2017 and 2018.

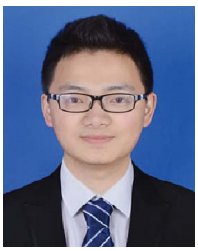

**Maodong Tang** received the B.Eng. degree in electrical engineering from the Nanjing University of Science and Technology, Nanjing, China, in 2019. He is currently pursuing the M.Eng. degree in electrical engineering with Southeast University, Nanjing.

His current research interest includes the control and modeling of dc microgrids.

**Ruoyu Yao** received the B.Eng. degree in electrical engineering from Northeast Electric Power University, Jilin, China, in 2019. She is currently pursuing the M.Eng. degree in electrical engineering with Southeast University, Nanjing, China.

Her current research interests include wireless power transfer and the stability analysis of dc microgrids.

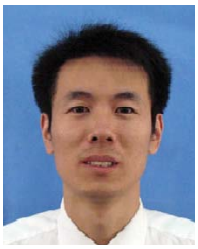

**Wu Chen** (Senior Member, IEEE) received the B.Eng., M.Eng., and Ph.D. degrees in electrical engineering from the Nanjing University of Aeronautics and Astronautics, Nanjing, China, in 2003, 2006, and 2009, respectively.

From 2009 to 2010, he was a Senior Research Assistant with the Department of Electronic Engineering, City University of Hong Kong, Hong Kong. From 2010 to 2011, he was a Postdoctoral Researcher with the Future Electric Energy Delivery and Management Systems Center, North Carolina State University, Raleigh. Since September 2011, he has been an Associate Research Fellow with the School of Electrical Engineering, Southeast University, Nanjing, China, where he has also been a Professor since 2016. His current research interests include soft-switching converters, power delivery, and power electronic system integration. He serves as an Associate Editor for the IEEE TRANSACTIONS ON INDUSTRIAL ELECTRONICS, the *Journal of Power Electronics*, and *CPSS Transactions on Power Electronics and Applications*.